Dalton Transactions

PAPER

View Article Online
View Journal | View Issue

Cite this: *Dalton Trans.*, 2017, **46**, 15458

X-ray crystallographic, luminescence and NMR studies of phenacyldiphenylphosphine oxide with the Ln(III) ions Sm, Eu, Gd, Tb and Dy†

Erin G. Leach,[a] Justin R. Shady,[a] Adam C. Boyden,[a] Anne-lise Emig,[a] Alyssa T. Henry,[b] Emily K. Connor,[b] Richard J. Staples,[c] Stephanie Schaertel,[a] Eric J. Werner[b] and Shannon M. Biros*[a]

Received 22nd July 2017,
Accepted 20th October 2017

DOI: 10.1039/c7dt02678a

rsc.li/dalton

We report here the characterization in solution (NMR, luminescence, MS) and the solid-state (X-ray crystallography, IR) of complexes between phenacyldiphenylphosphine oxide and five Ln(III) ions (Sm, Eu, Gd, Tb, Dy). Four single crystal X-ray structures are described here showing a 1 : 2 ratio between the Ln^{3+} ions Eu, Dy, Sm and Gd and the ligand, where the phosphine oxide ligands are bound in a monodentate manner to the metal center. A fifth structure is reported for the 1 : 2 $Eu(NO_3)_3$-ligand complex showing bidentate binding between the two ligands and the metal center. The solution coordination chemistry of these metal complexes was probed by ^1H, ^{13}C and ^{31}P NMR, mass spectrometry, and luminescence experiments. The title ligand has the capability to sensitize Tb^{3+}, Dy^{3+}, Eu^{3+} and Sm^{3+} leading to metal-centered emission in solutions of acetonitrile and methanol and in the solid state.

Introduction

Research into the chemistry of lanthanide (Ln) metals has generated recent interest due to their incorporation into advanced optical materials,[1–8] biosensors,[9–14] hybrid car batteries, and magnets that exploit their unique magnetic and photophysical properties.[6] The need for additional insight into factors that influence Ln coordination chemistry is further driven by the growing desire to recycle materials utilizing Ln metals (*e.g.*, hybrid car batteries, magnets, smart phones) combined with an increased focus on the purification of Ln metals from raw sources (ground ores and minerals).[15]

A well-known motif for chelating Ln metals is the carbamoylmethylphopshine oxide (CMPO) group. This motif is commonly used as a component of the TRUEX (transuranium extraction) process for nuclear waste remediation.[16] The coordination chemistry of the related aryl ketone derivative, **4**, has been investigated with both lanthanide and actinide metals by Platt and co-workers (Scheme 1).[17–19] We add to this body of work with five new crystal structures of β-ketophosphine oxide **4** complexed with Tb^{3+}, Eu^{3+}, Dy^{3+} and Gd^{3+}, as well as NMR and luminescence studies to probe the solution-state coordination chemistry.

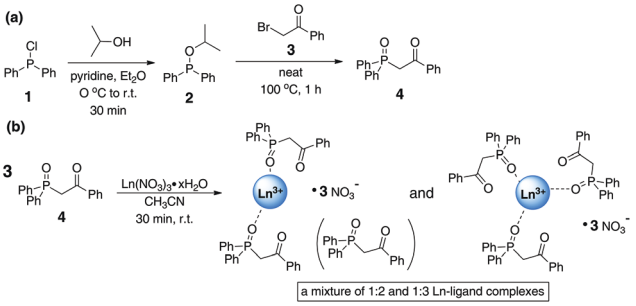

Scheme 1 Synthesis of (a) β-ketophopshine oxide **4** and (b) mixtures of 1 : 2 and 1 : 3 Ln-ligand complexes.

Experimental

General considerations

All chemicals (including deuterated solvents) were used as purchased from Sigma-Aldrich or Acros Chemicals and used without further purification. ^1H, ^{13}C and ^{31}P NMR spectral data were recorded on either a Jeol Eclipse 300 or Varian Inova

[a]*Department of Chemistry, Grand Valley State University, Allendale, MI 49401, USA. E-mail: biross@gvsu.edu; Fax: +1-616-331-3230; Tel: +1-616-331-8955*
[b]*Department of Chemistry, Biochemistry and Physics, The University of Tampa, 401 W. Kennedy Blvd., Tampa, FL 33606, USA*
[c]*Center for Crystallographic Research, Department of Chemistry, Michigan State University, 578 S. Shaw Lane, East Lansing, MI 48824, USA*

†Electronic supplementary information (ESI) available: Further details are given on the X-ray (all bond lengths and angles), NMR, IR and luminescence data (solid state emission spectra, lifetime decay curves, excitation and absorption spectra). CCDC 1484660–1484664 for **5–9**. For ESI and crystallographic data in CIF or other electronic format see DOI: 10.1039/c7dt02678a

400 FTNMR spectrophotometer, as stated. For ^{1}H and ^{13}C NMR spectra, chemical shifts are expressed as parts per million (δ) relative to $SiMe_4$ (TMS, δ = 0), and referenced internally with respect to the protio solvent impurity. For ^{31}P NMR spectra, chemical shifts are expressed as parts per million (δ) relative to H_3PO_4 (δ = 0). Both ^{13}C and ^{31}P NMR spectra were obtained as proton-decoupled data. IR spectra were acquired neat on a Jasco 4100 FTIR. Elemental (CHN) analyses were performed on a PerkinElmer 2400 Series II CHNS/O Analyzer or by Atlantic Microlab Inc., Norcross, GA; all CHN percentages calculated for lanthanide complexes assume 3 phosphine oxide ligands + $Ln(NO_3)_3$ + residual water/solvents as indicated. Mass spectrometry data were acquired on a Bruker Amazon speed ion trap instrument with electrospray ionization (ESI). Absorption spectra were acquired on a Shimadzu UV-2450 or Agilent 8453 UV-VIS spectrophotometer. Luminescence data were collected on either a Horiba Fluoromax 4 (emission spectra, luminescence lifetimes) or a Hitachi F-7000 spectrophotometer (77 K measurements, quantum yields).

Single crystal X-ray crystallography

Crystals suitable for X-ray diffraction were mounted on a nylon loop using a small amount of paratone oil. Data were collected using a Bruker CCD (charge coupled device) based diffractometer equipped with an Oxford Cryostream low-temperature apparatus operating at 173(2) K. Data were measured using omega and phi scans of 0.5° per frame. The total number of images was based on results from the program COSMO[20] where redundancy was expected to be 4.0 and completeness of 100% out to 0.83 Å. Cell parameters were retrieved using APEX II software[21] and refined using SAINT on all observed reflections. Data reduction was performed using the SAINT software,[22] which corrects for Lp. Scaling and absorption corrections were applied using SADABS[23] multi-scan technique, supplied by George Sheldrick. The structures were solved by the direct method using the SHELXS-97 program and refined by least squares method on F^2, SHELXL-2014,[24] which are incorporated in OLEX2.[25,26] All non-hydrogen atoms were refined anisotropically. Hydrogen atom locations were calculated by geometrical methods and refined as a riding model. The crystals used for the diffraction study showed no decomposition during data collection. Further crystallographic data and experimental details for structural analysis of all the complexes are summarized in Table 1, and selected bond lengths and angles with their estimated standard deviations are given in Tables 2 and 3. Complete tables for each structure reported here, along with diagrams depicting the thermal ellipsoids at 50%, are provided in the ESI.†

Photophysical studies

All luminescence studies were carried out with a 1 : 3 ratio of $Ln(NO_3)_3{\cdot}xH_2O$ to ligand **4** in chromasolv grade CH_3CN, HPLC grade CH_3OH or 99.5% atom %D CH_3OD. We prepared solutions of complexes for absorption, emission and excitation spectra by combining appropriate volumes of metal and ligand stock solutions to give an overall 2.0 mM concentration of Ln-**4** complex.

Quantum yields. Relative quantum yields of all Ln-**4** complexes were determined using the single-point method[27,28] with quinine sulfate as the reference fluorophore. Metal complex samples were diluted to 1.0×10^{-5} M in CH_3CN. Quinine sulfate solutions were diluted to 1.0×10^{-5} M in 0.1 M H_2SO_4. Integrated emission intensities (I) were collected with the Hitachi F-7000 instrument as noted above, exciting all samples at 300 nm with a scan speed of 240 nm min^{-1} and excitation/emission slit widths of 2.5 nm. Absorbance (A) values were recorded at 300 nm using an Agilent 8453 UV-Vis

Table 1 Crystal data and structure refinement for complexes **5–9**

Structure number	**5** $Eu(4)_2(NO_3)_3H_2O$	**6** $Gd(4)_2(NO_3)_3H_2O$	**7** $Tb(4)_2(NO_3)_3H_2O$	**8** $Dy(4)_2(NO_3)_3H_2O$	**9** $Eu(4)_2(NO_3)_3$
Empirical formula	$C_{40}H_{36}EuN_3O_{14}P_2$	$C_{40}H_{36}GdN_3O_{14}P_2$	$C_{40}H_{36}TbN_3O_{14}P_2$	$C_{40}H_{36}DyN_3O_{14}P_2$	$C_{40}H_{34}EuN_3O_{13}P_2{\cdot}(CHCl_3)_2$
CCDC number	1484663	1484664	1484662	1484660	1484661
Formula weight	996.62	1001.91	1003.58	1007.16	1217.34
Temperature/K	173(2)	173(2)	173(2)	173(2)	173(2)
Crystal system	Triclinic	Triclinic	Triclinic	Triclinic	Triclinic
Space group	$P\bar{1}$	$P\bar{1}$	$P\bar{1}$	$P\bar{1}$	$P\bar{1}$
a/Å	11.2311(19)	11.23800(10)	11.2287(12)	11.2313(7)	12.5305(12)
b/Å	11.6325(19)	11.6353(2)	11.6265(12)	11.6143(7)	14.0929(14)
c/Å	18.480(3)	18.4819(2)	18.433(2)	18.4094(11)	16.2116(16)
α/°	72.083(2)	72.0301(6)	72.0460(10)	72.0480(10)	71.5480(10)
β/°	75.706(2)	75.7452(6)	75.8340(10)	75.8590(10)	80.1730(10)
γ/°	66.718(2)	66.7376(6)	66.6960(10)	66.6400(10)	72.0490(10)
Volume/Å^3	2088.3(6)	2090.38(5)	2081.6(4)	2076.6(2)	2575.0(4)
Z	2	2	2	2	2
Reflections collected	21 495	30 211	34 436	29 641	51 489
Independent reflections	7660 [R_{int} = 0.0483, R_{sigma} = 0.0523]	7956 [R_{int} = 0.0389, R_{sigma} = 0.0359]	7587 [R_{int} = 0.0518, R_{sigma} = 0.0428]	7902 [R_{int} = 0.0512, R_{sigma} = 0.0508]	9820 [R_{int} = 0.1507, R_{sigma} = 0.1278]
Final R indexes [$I \geq 2\sigma(I)$]	R_1 = 0.0452, wR_2 = 0.1178	R_1 = 0.0242, wR_2 = 0.0603	R_1 = 0.0293, wR_2 = 0.0618	R_1 = 0.0321, wR_2 = 0.0656	R_1 = 0.0730, wR_2 = 0.1540
Final R indexes [all data]	R_1 = 0.0511, wR_2 = 0.1246	R_1 = 0.0257, wR_2 = 0.0613	R_1 = 0.0371, wR_2 = 0.0654	R_1 = 0.0435, wR_2 = 0.0702	R_1 = 0.1287, wR_2 = 0.1769

Table 2 Selected bond distances (Å) for Ln-**4** structures **5–9** reported here, as well as the $Er(NO_3)_3\mathbf{4}_2(H_2O)$[17] (**10**) and $Ce(NO_3)_3\mathbf{4}_3$[18] (**11**) data reported previously

	Ten-coordinate Ln(III)		Nine-coordinate Ln(III)				
	11[18] $Ce(\mathbf{4})_3(NO_3)_3$	**9** $Eu(\mathbf{4})_2(NO_3)_3$	**5** $Eu(\mathbf{4})_2(NO_3)_3H_2O$	**6** $Gd(\mathbf{4})_2(NO_3)_3H_2O$	**7** $Tb(\mathbf{4})_2(NO_3)_3H_2O$	**8** $Dy(\mathbf{4})_2(NO_3)_3H_2O$	**10**[17] $Er(\mathbf{4})_2(NO_3)_3H_2O$
Monodentate ligand							
Ln–O1(P)	2.401	—	2.306(3)	2.2914(16)	2.281(2)	2.264(2)	2.246
Ln–O1a(P)	2.410	—	2.301(3)	2.2882(15)	2.273(2)	2.263(2)	2.253
Bidentate ligand							
Ln–O1(P)	2.446	2.345(5)	—	—	—	—	—
Ln–O2(C)	2.609	2.496(6)	—	—	—	—	—
Ln–O1a(P)	—	2.372(5)	—	—	—	—	—
Ln–O2a(C)	—	2.536(6)	—	—	—	—	—
Water and bidentate nitrates							
Ln–O1w	—	—	2.392(3)	2.3739(15)	2.358(2)	2.344(2)	2.323
Ln–O3b(N)	2.630	2.620(5)	2.486(3)	2.4797(16)	2.470(2)	2.453(2)	2.431
Ln–O4b(N)	2.623	2.535(5)	2.475(4)	2.4608(19)	2.445(3)	2.429(3)	2.410
Ln–O3c(N)	2.672	2.494(6)	2.482(3)	2.4827(18)	2.464(2)	2.443(2)	2.420
Ln–O4c(N)	2.526	2.454(6)	2.513(3)	2.5068(18)	2.488(2)	2.478(3)	2.443
Ln–O3d(N)	2.753	2.605(6)	2.500(3)	2.5007(17)	2.485(2)	2.477(2)	2.472
Ln–O4d(N)	2.580	2.504(5)	2.498(3)	2.4908(17)	2.472(2)	2.458(3)	2.432

Table 3 Selected bond angles (°) for Ln-**4** structures **5–9** reported here, as well as the $Ce(NO_3)_3\mathbf{4}_3$[18] and $Er(NO_3)_3\mathbf{4}_2(H_2O)$[17] data reported previously

	Ten-coordinate Ln(III)		Nine-coordinate Ln(III)				
	11[18] $Ce(\mathbf{4})_3(NO_3)_3$	**9** $Eu(\mathbf{4})_2(NO_3)_3$	**5** $Eu(\mathbf{4})_2(NO_3)_3H_2O$	**6** $Gd(\mathbf{4})_2(NO_3)_3H_2O$	**7** $Tb(\mathbf{4})_2(NO_3)_3H_2O$	**8** $Dy(\mathbf{4})_2(NO_3)_3H_2O$	**10**[17] $Er(\mathbf{4})_2(NO_3)_3H_2O$
Monodentate ligand							
O1–Ln–O1a	83.724	—	84.39(11)	84.18(6)	84.21(8)	84.20(8)	83.718
O1–Ln–O3b	72.096	—	72.52(10)	72.49(6)	72.63(8)	72.62(8)	73.480
O1–Ln–O3d	66.575	—	75.64(12)	75.77(6)	75.70(8)	75.95(9)	75.938
O1–Ln–O4d	77.661	—	80.04(12)	79.82(6)	80.14(8)	80.57(9)	80.608
O1–Ln–O1w	—	—	82.81(11)	83.00(6)	83.04(8)	83.30(8)	83.883
O1a–Ln–O3b	74.434	—	79.20(10)	78.95(6)	78.95(8)	78.92(8)	78.982
O1a–Ln–O4b	88.035	—	80.86(12)	81.04(7)	80.94(9)	81.20(9)	81.505
O1a–Ln–O4c	79.816	—	77.56(11)	77.69(6)	77.41(8)	77.22(8)	77.259
O1a–Ln–O4d	73.151	—	76.23(11)	76.35(6)	76.47(8)	76.68(8)	76.674
O1a–Ln–O1w	—	—	152.05(11)	151.68(6)	151.55(8)	151.60(9)	151.959
Bidentate ligand							
O1–Ln–O2	68.125	72.03(18)	—	—	—	—	—
O1a–Ln–O2a	—	71.60(18)	—	—	—	—	—
O1–Ln–O3d	74.482	69.02(17)	—	—	—	—	—
O2–Ln–O4b	74.084	73.31(19)	—	—	—	—	—
O1a–Ln–O3b	—	71.19(18)	—	—	—	—	—
O2a–Ln–O4d	—	73.41(17)	—	—	—	—	—
Water and bidentate nitrates							
O3b–Ln–O4b	47.266	49.07(18)	51.14(11)	51.62(6)	51.90(8)	52.14(9)	51.975
O3c–Ln–O4c	48.069	51.8(2)	50.83(11)	50.98(6)	51.35(8)	51.52(8)	52.023
O3d–Ln–O4d	47.542	49.22(17)	50.89(10)	51.07(5)	51.35(7)	51.46(8)	51.719
O1w–Ln–O3b	—	—	73.29(10)	73.14(6)	72.99(8)	73.04(8)	73.405
O1w–Ln–O4b	—	—	85.66(12)	85.36(6)	85.43(8)	85.10(9)	85.305
O1w–Ln–O3c	—	—	72.57(11)	72.48(6)	72.44(8)	72.21(9)	71.475
O1w–Ln–O3d	—	—	74.70(10)	74.76(6)	74.63(8)	74.55(8)	74.023

spectrophotometer. The quantum yield of each Ln-**4** (Φ_x) complex was calculated using the following equation:

$$\Phi_x = \frac{\Phi_r I_x A_r n_x^2}{I_r A_x n_r^2}$$

where subscripts r and x denote the quinine sulfate reference standard and Ln-**4** sample, respectively, n denotes the refractive index of each solution (n_r = 1.3340 and n_x = 1.344), and Φ_r is taken as 0.54. The relative quantum yield of each Ln-**4** complex was measured in triplicate to yield the reported average values and standard deviations.

Ligand triplet state energy. The triplet state energy of compound **4** in acetonitrile was determined by recording emission spectra of the 1 : 3 $Gd(NO_3)_3$-**4** complex at 77 K. Separate stock solutions of the ligand and metal nitrate salt were prepared and combined to give a solution of the 1 : 3 (M : L) complex at

1.0×10^{-4} M. Low temperature spectra were recorded with the Hitachi F-7000 spectrophotometer running in both fluorescence and phosphorescence mode (scan rate = 240 nm min^{-1}, λ_{ex} = 350 nm, SW = 5 nm for fluorescence and scan rate = 240 nm min^{-1}, λ_{ex} = 350 nm, SW = 10 nm for phosphorescence), with phosphorescence emission being collected following a 1 ms delay time after initial excitation. The triplet state energy value was obtained from deconvolution of the phosphorescence spectrum into its Gaussian components (OriginPro 2017). The peak corresponding to the highest energy vibrational level obtained from deconvolution was used to calculate the ligand triplet state energy.[29]

Synthesis

$iPrOPPh_2$ in diethyl ether (2). The procedure of Shintou and co-workers[30] was followed for the preparation of the iso-propoxydiphenyl phosphine **2**; we varied only the isolation procedure, which is described here. After the pyridinium hydrochloride salt was removed using a Hirsch funnel, the solid was rinsed with diethyl ether. The filtrate was concentrated on a rotary evaporator under reduced pressure, with the water bath at room temperature, until the majority of the solvent was removed. If care is not taken with this step it is possible to evaporate the desired product along with solvent diethyl ether. The crude reaction mixture was analyzed by ^{1}H NMR, and the relative amount of product to solvent ether was determined by integration. If remaining pyridinium chloride was detected in the product, it was precipitated out by placing the solution in the refrigerator overnight. The product was then decanted the following day and reanalyzed by ^{1}H NMR. The resultant iso-propoxydiphenylphosphine **2** is stable for months if stored in the refrigerator as a solution in diethyl ether. Typically, we carried forward a ~65% solution of $iPrOPPh_2$ in diethyl ether to the procedure described below.

Phenacyldiphenylphosphine oxide (4). Compound **4** was prepared in two steps following slightly modified procedures of Böhmer[31] and Gandelman.[32] Isopropoxy ether **2** (as an ethereal solution, typically 5–10 gram scale) and 2-bromoacetophenone **3** (10% molar excess) were mixed, without additional solvent, in an open 50 mL round bottom flask at room temperature. After approximately 5–10 minutes, the reaction mixture warmed rapidly and a gaseous byproduct was evolved. When the reaction had cooled to room temperature, the mixture was heated to 100 °C for thirty minutes at which point the solution became quite viscous. The reaction mixture was allowed to cool to room temperature, and the viscous oil was dissolved in $CHCl_3$ (30 mL) and added drop wise to a solution of saturated $NaHCO_3$ (45 mL). The solution was transferred to a separatory funnel, and the organic layer was drained off. The aqueous phase was extracted with $CHCl_3$ (2 × 30 mL). The combined chloroform layers were washed with saturated sodium bicarbonate (2 × 25 mL), brine (1 × 25 mL), dried over $MgSO_4$ and concentrated under reduced pressure. The resulting orange-red oil was placed under high vacuum overnight to remove any remaining volatile impurities. The product was purified by trituration with Et_2O and EtOAc (three times each) to give an off-white powder in reasonable yield (2.89 g, 56% from 3.18 g starting bromoacetophenone). ^{1}H NMR ($CDCl_3$, 300 MHz) δ: 7.98 (m, 2H), 7.83–7.76 (m, 4H), 7.54–7.38 (m, 9H), 4.12 (d, J_{P-H} = 15 Hz, 2H); ^{13}C NMR ($CDCl_3$, 100 MHz): δ 193.0 (d, J_{P-C} = 5.9 Hz, C═O), 137.2 (s), 133.8 (m), 132.7 (s), 132.4 (m), 131.6 (s), 131.3 (m), 129.4 (s), 128.8 (m), 43.4 (d, J_{P-C} = 58 Hz, CH_2); ^{31}P NMR ($CDCl_3$, 121 MHz) δ: 28.1; ^{1}H NMR (CD_3CN, 400 MHz): δ 7.98 (m, 2H), 7.80 (m, 4H), 7.40–7.60 (m, 9H), 4.25 (d, J_{P-H} = 14.8 Hz, 2H, CH_2); ^{13}C NMR (CD_3CN, 100 MHz): δ 194.1 (d, J_{C-P} = 6.2 Hz, C═O), 138.3 (s), 134.1 (d, J_{C-P} = 134 Hz), 131.7 (m), 130.0 (s), 129.6 (m), 129.3 (m), 40.5 (d, J_{C-P} = 60.1 Hz, CH_2); ^{31}P NMR (CD_3CN, 121 MHz): δ 26 (s); FT-IR ν (cm^{-1}): 1680 (C═O), 1440 (CH_2), 1179 (P═O); UV-VIS (6.0 mM, CH_3CN): λ_{max} = 317 nm.

Metal–ligand complex synthesis. General procedure for $Ln(NO_3)_3$ (Ln = Sm, Eu, Tb, Dy) complexes described here. Phosphine oxide **4** (50 mg, 0.156 mmol) and 1/3 molar equivalent of $Ln(NO_3)_3{\cdot}6H_2O$ were dissolved in acetonitrile (~15 mL) and stirred at room temperature for thirty minutes. The volatiles were removed under reduced pressure, and the resultant clear film was triturated two to three times with diethyl ether to give off-white powders. The characterization data for each of the metal–ligand complexes are given below.

Sm-$(4)_3(NO_3)_3$. ^{1}H NMR (CD_3CN, 400 MHz): δ 8.28 (m, 4H), 7.72 (m, 2H), 7.57 (m, 3H), 7.34 (m, 6H), 4.93 (d, J_{P-H} = 14.8 Hz, 2H, CH_2); ^{13}C NMR (CD_3CN, 100 MHz): δ 193.8 (d, J_{P-C} = 5.6 Hz, C═O), 136.5 (d, J_{P-C} = 3.6 Hz), 134.4 (s), 133.2 (s), 131.6 (d, J_{P-C} = 10.7 Hz), 130.3 (d, J_{P-C} = 107 Hz), 129.1 (m), 42.9 (d, J_{P-C} = 68.2 Hz, CH_2); ^{31}P NMR (CD_3CN, 162 MHz): δ 35 (broad s); FT-IR ν (cm^{-1}): 2869 (CH), 1677 (C═O), 1138 (P═O); ESI-LRMS (M^+, m/z): calcd for $Sm(C_{20}H_{17}O_2P)_3(NO_3)_2$: 1236.2, found 1236.3; calcd for $Sm(C_{20}H_{17}O_2P)_2(NO_3)_2$: 916.1, found 916.1; anal. calcd for $Sm(C_{20}H_{17}O_2P)_3(NO_3)_3$ (found): C, 55.55 (55.47); H, 3.96 (4.06); N, 3.24 (3.27).

Eu-$(4)_3(NO_3)_3$. FT-IR ν (cm^{-1}): 1676 (C═O), 1138 (P═O); ESI-LRMS (M^+, m/z): calcd for $Eu(C_{20}H_{17}O_2P)_3(NO_3)_2$: 1235.2, found 1235.1; calcd for $Eu(C_{20}H_{17}O_2P)_2(NO_3)_2$: 915.1, found 915.1; anal. calcd for $Eu(C_{20}H_{17}O_2P)_3(NO_3)_3(CH_3CN)(H_2O)_3$ (found): C, 53.42 (53.46); H, 4.34 (3.90); N, 4.02 (3.71).

Tb-$(4)_3(NO_3)_3$. FT-IR ν (cm^{-1}): 1677 (C═O), 1141 (P═O); ESI-LRMS (M^+, m/z): calcd for $Tb(C_{20}H_{17}O_2P)_3(NO_3)_2$: 1243.2, found 1243.3; calcd for $Tb(C_{20}H_{17}O_2P)_2(NO_3)_2$: 923.6, found 923.6; anal. calcd for Tb $(C_{20}H_{17}O_2P)_3(NO_3)_3(CH_3CN)(H_2O)_4$ (found): C, 52.48 (52.07); H, 4.40 (3.82); N, 3.95 (3.91).

Dy-$(4)_3(NO_3)_3$. FT-IR ν (cm^{-1}): 1676 (C═O), 1140 (P═O); ESI-LRMS (M^+, m/z): calcd for $Dy(C_{20}H_{17}O_2P)_3(NO_3)_2$: 1248.2, found 1248.4; calcd for $Dy(C_{20}H_{17}O_2P)_2(NO_3)_2$: 928.1, found 928.3; anal. calcd for Dy $(C_{20}H_{17}O_2P)_3(NO_3)_3(CH_3CN)(H_2O)_2$ (found): C, 53.71 (53.46); H, 4.22 (3.90); N, 4.04 (3.71).

Results and discussion

Synthesis of ligand and Ln-ligand complexes

Phosphine oxide ligand **4** was readily prepared in two steps using Arbuzov chemistry (Scheme 1a).[31] Diphenylchloro-

phosphine **1** was transformed into the isopropoxyether **2**,[30] then heated with 2-bromoacetophenone **3** to give the β-ketophosphine oxide **4** as a beige solid after successive triturations with diethyl ether and ethyl acetate. Lanthanide complexes (Ln = Eu, Sm, Tb, Dy) were then prepared by stirring three molar equivalents of **4** to one molar equivalent lanthanide nitrate hydrate in acetonitrile for thirty minutes. Isolation of the complexes was achieved by removal of the volatiles and trituration with diethyl ether to give off-white powders.

Single crystal X-ray diffraction studies

Although all metal–ligand complexes were prepared with a 1 : 3 $Ln(NO_3)_3$-**4** ratio, all single crystal products analyzed by X-ray diffraction had a 1 : 2 metal–ligand ratio. Platt and co-workers also observed this coordination stoichiometry with complexes of ligand **4** with $Er(NO_3)_3$ [17] and $UO_2(NO_3)_2$.[19] For the larger lanthanide $Ce(NO_3)_3$,[17,18] the X-ray structure of a 1 : 3 metal–ligand complex was reported. Here we add five new $Ln(NO_3)_3$-**4** structures to this series, where Ln = Eu, Tb, Gd and Dy. Four of these have the same coordination geometry as Platt's Er^{3+} complex (**5–8**, Fig. 1a),[17] with two phosphine oxide ligands each bound to the Ln center in a monodentate manner *via* the phosphoryl oxygen. The inner coordination sphere of these complexes also contains three bidentate nitrate groups and one water molecule. The bound aqua ligand is engaged in an intramolecular hydrogen bond with the carbonyl oxygen of a metal bound ligand.

The fifth structure reported here is a 1 : 2 metal–ligand complex with $Eu(NO_3)_3$, however in this case both organic ligands bind the metal in a bidentate manner with expulsion of the inner-sphere aqua ligand (**9**, Fig. 1b). Additionally, three molecules of solvent chloroform are present in the asymmetric unit. One of these $CHCl_3$ molecules was ordered, while the second $CHCl_3$ molecule was disordered and was modeled with 50% occupancies over two orientations. Electron density corresponding to, what we believe, is a third $CHCl_3$ molecule was severely disordered and located on a symmetry center with coordinates of [0.000, 0.000, 0.500]. This space has a volume of 147.9 Å^3 and contains 57.7 electrons. This disordered electron density was removed using the BYPASS[33] instructions as implemented in Olex2.[25,26]

Crystal structure and refinement data for all new structures **5–9** reported here are given in Table 1, and pertinent bond lengths and angles for all Ln-**4** structures (including those of Platt and co-workers) are given in Tables 2 and 3 respectively. The atom numbering scheme for all crystal structures is shown in Fig. 2. Additional structural and experimental details regarding the crystallographic data can be found in the ESI.†

For the nine-coordinate structures **5–8** and **10** where ligand **4** is bound in a monodentate manner, the P═O···Ln^{3+} bond lengths decrease as the Ln^{3+} ionic radii decrease. Similarly, the nitrate and water O···Ln^{3+} bond lengths also follow this trend. The bond angles between the nine-coordinated ligands, however, show little change as the Ln^{3+} ionic radii decreases across the row.

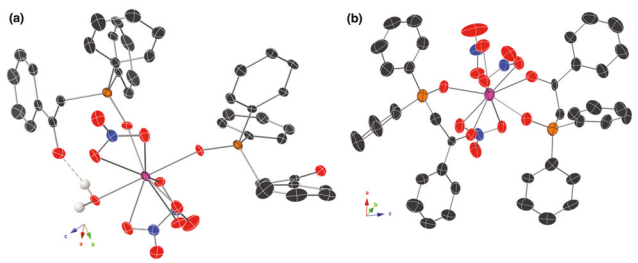

Fig. 1 (a) Representative X-ray crystal structure of the nine-coordinate $Ln(NO_3)_3$**4**$_2(H_2O)$ complex **5** where Ln = Eu (the isostructural Ln = Dy, Gd, Sm structures are shown in the ESI†); (b) X-ray crystal structure of the ten-coordinate $Eu(NO_3)_3$**4**$_2(CHCl_3)_2$ complex **9** (solvent $CHCl_3$ molecules have been omitted for clarity). Structures are shown with 30% probability ellipsoids using standard CPK colors, the Eu(III) atom is colored magenta, non-polar hydrogen atoms have been omitted for clarity, and a hydrogen bond is shown as a dashed line.

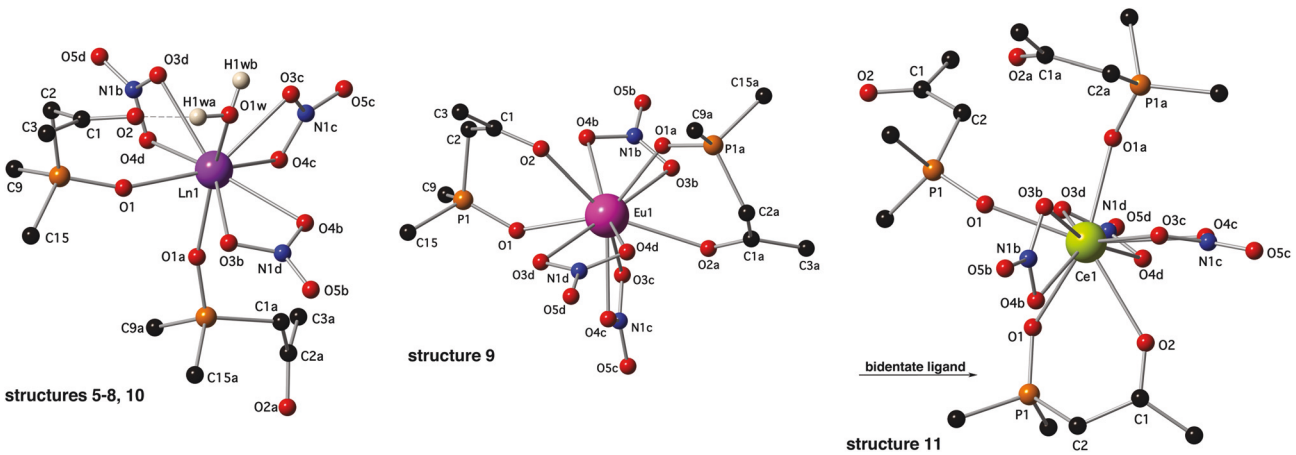

Fig. 2 Atom numbering scheme used in Tables 2 and 3 for structures **5–8** and **10** [$Ln(NO_3)_3$**4**$_2(H_2O)$ where Ln = Eu, Gd, Dy, Tb, Er[17]], **9** [$Eu(NO_3)_3$**4**$_2$] and **11** [$Ce(NO_3)_3$**4**$_3$].[18] Pendant phenyl rings and nonpolar hydrogen atoms have been omitted for clarity.

The two ten-coordinate structures, **9** and **11**, also show a decrease in O···Ln^{3+} bond lengths from the Ce^{3+} to the Eu^{3+} complex. For the complexes containing bidentate phosphine oxide ligands, the P═O···Ln^{3+} bond is shorter than the C═O···Ln^{3+} bond, which is consistent with a stronger interaction between the more polarized phosphine oxide group and the Ln^{3+} ion.

Some additional structural information can be gleaned by comparing the ten-coordinate Eu^{3+} and the nine-coordinate Eu^{3+} structures (**9** *vs.* **5**). As noted above, in the ten-coordinate structure **9** both phosphine oxide ligands are bound to the Eu^{3+} center in a bidentate manner, while in the nine-coordinate structure **5** both ligands bind only through the phosphine oxide group. The P═O···Eu^{3+} and nitrate NO···Eu^{3+} bond lengths are longer in the bidentate ten-coordinate structure (with the exception of one NO···Eu^{3+} bond), which is consistent with the larger ionic radius for a ten-coordinate Eu^{3+} center. The bond angles between the nitrate ligands are again similar between the nine- and ten-coordinate structures.

The structural features observed using X-ray diffraction were also confirmed with peaks in the FT-IR spectra of the $Ln(NO_3)_3$-**4** complexes (Table 4). In the neat IR spectra of the lanthanide complexes described here, broad peaks for the C═O and P═O stretches were observed for the complexes *versus* free ligand. The stretches for both groups shift to lower wavenumbers upon complexation with the Ln(III) metal (Ln = Eu, Tb, Dy, Sm). The C═O stretch shifts only ~5 cm^{-1} while the P═O stretch shifts ~35 cm^{-1}, indicating that the phosphine oxide is engaged in a dative bond with the lanthanide metal center. The small shift observed for the carbonyl stretch may be due to the formation of a hydrogen bond with a metal-bound water molecule, as observed in the crystal structures, *versus* coordination with the Ln.

The IR data also support the presence of only inner sphere, bidentate nitrate groups in all Ln-ligand complexes studied. Ionic outer sphere nitrate ions typically show bands around 1390 cm^{-1}, while inner sphere nitrate groups show bands around 1450 cm^{-1} (ν(N═O)) and ~1300 cm^{-1} ($\nu(NO_2)$).[34–36] In the four Ln-complexes studied here, no stretches for purely ionic nitrate anions were observed. For the inner sphere nitrate groups, bands were observed at ~1460 cm^{-1} and ~1290 cm^{-1}, with peak separation values of greater than 140 cm^{-1}. This large peak separation suggests the presence of inner sphere, bidentate nitrate groups in the solid state. This analysis is consistent with the X-ray data reported here as well as the IR data (obtained with KBr discs) reported by Babecki and co-workers.[17]

Solution studies with MS and NMR

Although the X-ray diffraction data from the new $Ln(NO_3)_3$-**4** complexes described in this paper reflect a 1 : 2 stoichiometry between $Ln(NO_3)_3$ and ligand **4** in the solid state, we were curious if complexes with a 1 : 3 stoichiometry were present in solution. To test this, we analyzed acetonitrile solutions of 1 : 3 $Ln(NO_3)_3$-**4** complexes in the gas phase using ESI-MS (Ln = Tb, Eu, Dy, Sm). The mass spectrum of each $Ln(\mathbf{4})_3(NO_3)_3$ complex in acetonitrile displays prominent peaks corresponding to $[Ln\text{-}\mathbf{4}_2(NO_3)_2]^+$ and $[Ln\text{-}\mathbf{4}_3(NO_3)_3]^+$ complexes, suggesting that both stoichiometries are present in solution (spectra shown in ESI†). Based on this result, we carried out all solution studies with three equivalents of ligand **4** to each $Ln(NO_3)_3$. This stoichiometry should favor the presence of 1 : 2 and 1 : 3 $Ln(NO_3)_3$-ligand complexes as the dominant species in solution. We expect that complexes with a 1 : 1 or 1 : 4 $Ln(NO_3)_3$-ligand stoichiometry are not present in appreciable amounts in solution.

With the results from our MS analysis in hand, we investigated the structure of the complexes in solution using NMR. Unfortunately, the signals of the Eu^{3+}, Dy^{3+} and Tb^{3+} complexes were severely broadened in the ^{1}H NMR spectra and were uninterpretable. The Sm^{3+} complex, however, gave signals that were interpretable in the ^{1}H, ^{31}P and ^{13}C NMR spectra. The ^{1}H NMR spectrum of the $Sm(NO_3)_3$-**4** complex with three equivalents of ligand **4** in CD_3CN is shown in Fig. 3a. Most notably, the signal corresponding to the hydrogen atoms of the methylene group of the ligand is shifted downfield ~0.5 ppm relative to the ligand alone, supporting complexation with the Sm^{3+} metal center in solution. Only one signal for the hydrogen atoms of this methylene group is observed, indicating that this spectrum shows time-averaged signals and that exchange between free ligand and all possible metal–ligand complex stoichiometries (*e.g.* 1 : 2 and 1 : 3 Ln-**4** ratios) occurs quickly on the NMR time scale.

The 1 : 3 $Sm(NO_3)_3$-**4** complexes also gave interpretable ^{13}C and ^{31}P NMR spectra in CD_3CN. The signal corresponding to the phosphorus atom resonates downfield relative to the ligand alone and is broadened, indicating that the phosphine oxide group is coordinated to the Sm^{3+} metal ($\Delta\delta$ = +9 ppm). The ^{13}C NMR of the 1 : 3 $Sm(NO_3)_3$-CMPO complex (Fig. 3b) shows a sharp signal for the carbonyl carbon that is shifted slightly upfield relative to the signal for the carbonyl carbon of the free ligand ($\Delta\delta$ = −0.3 ppm). The signal corresponding to the carbon atom of the methylene group of **4** in the metal complex, however, is shifted downfield 2.4 ppm relative to that of the free ligand. These results indicate that, in acetonitrile-

Table 4 Infrared absorption bands (cm^{-1}) for ligand **4** and the complexes with $Ln(NO_3)_3$ (Ln = Sm, Eu, Dy, Tb)

	ν(C═O)	ν(P═O)	ν(N═O)	$\nu_a(NO_2)$	$\nu_s(NO_2)$	ν(NO)
4	1680	1179	—	—	—	—
$Sm(NO_3)_3(\mathbf{4})_3$	1677	1138	1464	1291	1029	817
$Eu(NO_3)_3(\mathbf{4})_3$	1676	1138	1467	1290	1028	816
$Dy(NO_3)_3(\mathbf{4})_3$	1676	1140	1472	1292	1030	814
$Tb(NO_3)_3(\mathbf{4})_3$	1677	1143	1458	1294	1030	815

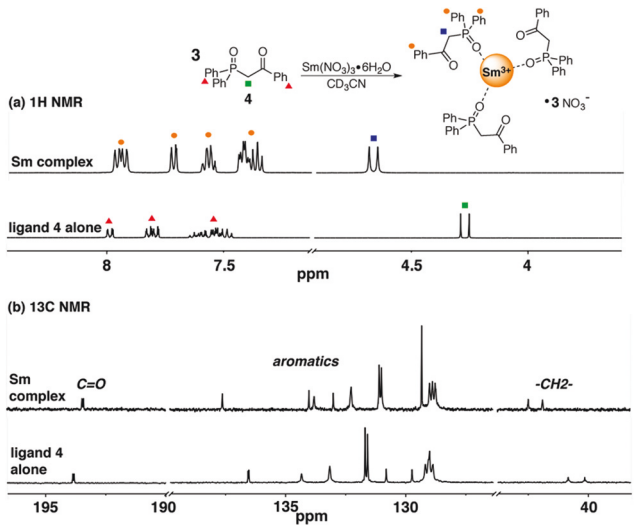

Fig. 3 (a) ^{1}H NMR spectrum (400 MHz, CD_3CN) of (bottom) **4** alone, and (top) the 1 : 3 $Sm(NO_3)_3$-**4** complex; (b) ^{13}C NMR spectrum (100 MHz, CD_3CN) of (bottom) **4** alone and (top) the 1 : 3 $Sm(NO_3)_3$-**4** complex.

d_6, coordination of ligand **4** to the Sm^{3+} metal center occurs primarily *via* the phosphine oxide group. This conclusion is supported by the solid state data discussed above.

To support our emission spectroscopy studies (*vide infra*), we also investigated the effect of concentration on complex structure using ^{1}H NMR spectroscopy. A series of ^{1}H NMR spectra were acquired with successively decreasing concentrations of a solution containing three equivalents of ligand **4** to $Sm(NO_3)_3$ in CD_3CN (Fig. 4). Our goal with this experiment was to find the lower concentration limit for complex formation in acetonitrile, so we could be assured that at the concentrations we were analyzing for the measurement of quantum yields (10^{-5} M) appreciable amounts of the complex was present. The ^{1}H NMR spectra shown in this figure are quite noisy due to the dilute samples we were analyzing; the top spectrum (10^{-6} M complex) required 48 hours of acquisition time at 300 MHz.

Down to a concentration of 10^{-4} M of the solution described above, the signal corresponding to the hydrogen atoms of the methylene group of ligand **4** resonates at 4.4 ppm, which is consistent with the chemical shift of bound ligand that was observed from the higher concentration solutions shown in Fig. 3. However, upon further dilution of this sample the signal corresponding to the hydrogen atoms of the methylene group begins to shift upfield until at ~10^{-6} M it returns to the chemical shift of the free ligand. This experiment demonstrates that the $Sm(NO_3)_3$-**4** complexes present in solution are stable down to concentrations of ~10^{-5} M in acetonitrile, which is the lowest concentration that was analyzed for the determination of quantum yields (*vide infra*).

Luminescence properties

Since its discovery in 1942 by Weissman,[37] the ability to sensitize lanthanide luminescence with a bound organic ligand has received a tremendous amount of attention due to the unique characteristics of metal-centered emission.[6] With the exception of La(III) and Lu(III), lanthanide metals luminesce with

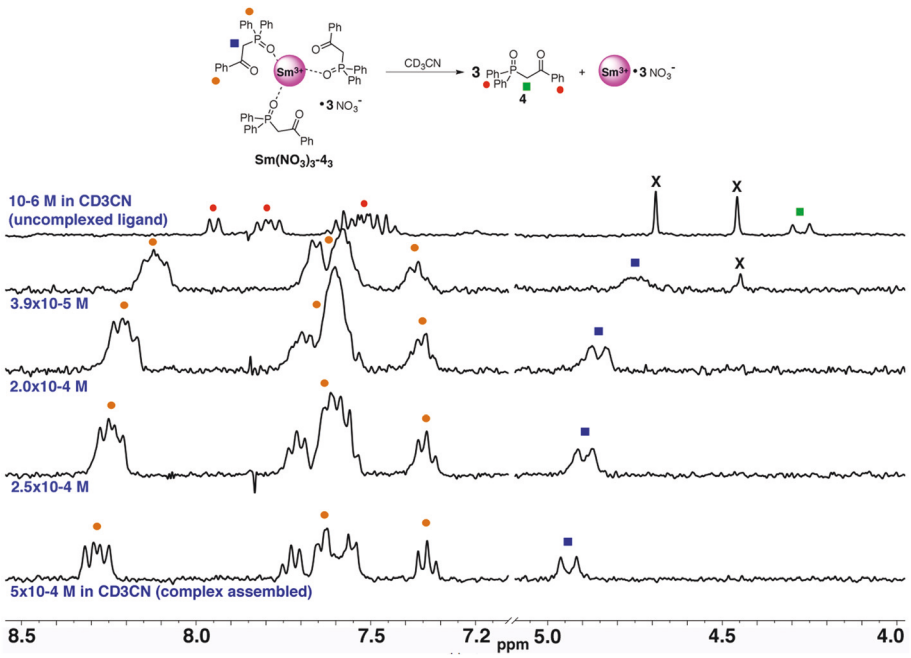

Fig. 4 ^{1}H NMR spectra from the sequential dilution of a solution containing three equivalents ligand **4** to $Sm(NO_3)_3$ in CD_3CN (300 MHz). Signals labeled with blue squares and orange circles belong to the assembled complex; signals labeled with green squares and red circles belong to the dissociated complex; *X* denotes an impurity detectable only at low concentrations of ligand.

narrow emission bands (~10 nm) at wavelengths in the UV, visible and near-IR regions. The Ln excitation process requires a parity forbidden f → f transition, and this process can be facilitated by a bound organic ligand having an excited triplet state with an energy level slightly greater than that of the Ln^{3+} ion of interest (ΔE = 2000–4000 cm^{-1}). Fig. 5 shows an abbreviated Jablonski diagram describing this "antenna effect".

Since compounds containing aryl-substituted carbonyl groups have been reported to act as antennas for metal centered luminescence,[38] we investigated the ability of β-ketophosphine oxide **4** to promote this process. Our studies encompassed $Ln(NO_3)_3$-**4** complexes composed of four of the lanthanide nitrates with emission in the visible region: Eu^{3+}, Tb^{3+}, Sm^{3+}, and Dy^{3+}. We again used three equivalents of ligand **4** to ensure complete metal complexation and to favor the presence of complexes with 1 : 2 and 1 : 3 Ln-ligand stoichiometry in solution. The absorption and excitation spectra of the $Dy(NO_3)_3$-**4** complex with three equivalents of **4** in acetonitrile are shown in Fig. 6. The absorption spectrum of ligand **4** alone is broad with a maximum at 317 nm, and in the presence of $Dy(NO_3)_3$ this maximum is shifted to 294 nm. The excitation spectrum of the $Dy(NO_3)_3$-**4** complex (monitored at 478 nm) has a maximum at 322 nm, and is similar in shape to the absorption spectrum with a slight red shift. These features support the complexation of $Dy(NO_3)_3$ in solution by ligand **4**, as well as the sensitization of metal centered emission. The absorption and excitation spectra of the other three complexes are similar in all respects to the Dy^{3+} complex, and are shown in the ESI.†

Emission spectra for solutions with a 3 : 1 ligand **4** to $Ln(NO_3)_3$ stoichiometry in acetonitrile are shown in Fig. 7 with

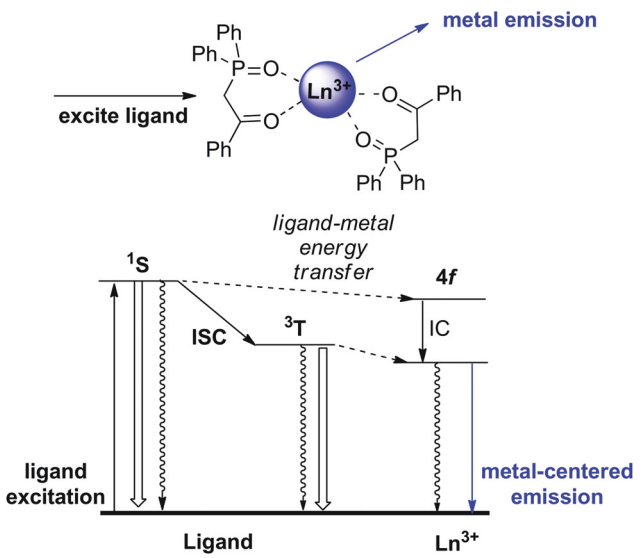

Fig. 5 Schematic of possible mechanisms for the "antenna effect" for luminescent lanthanide complexes with a simplified Jablonski diagram; open arrows = fluorescence (from ^1S) and phosphorescence (from ^3T) of ligand, ISC = inter-system crossing, IC = internal conversion, squiggly arrows = non-radiative decay pathways from ligand or metal.

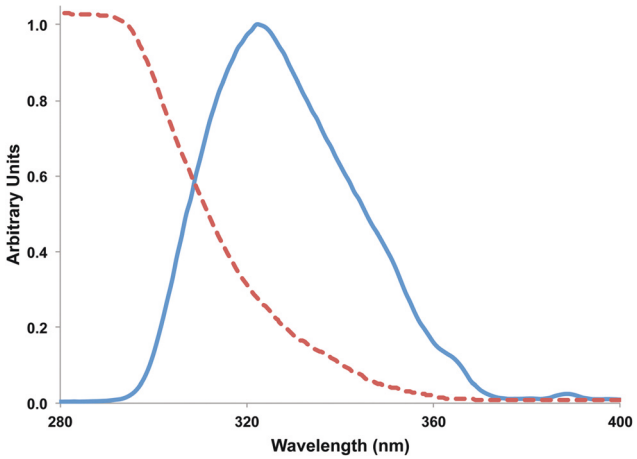

Fig. 6 Absorption (red dashed) and excitation (blue solid) spectra of the $Dy(NO_3)_3$-**4** complex with three equivalents of ligand **4** in acetonitrile (2.0 mM complex concentration, λ_{em} monitored at 478 nm, 2.0 nm emission and excitation slits). Both absorption and excitation spectra have been normalized to have their peaks at 1 arbitrary unit for ease of comparison.

excitation at 350 nm, along with photos of the emission from the solid state. Characteristic emission bands[11] are seen for each of the Ln-**4** complexes in acetonitrile (complex concentration 2.0 mM). Emission of the Tb^{3+} complex is the brightest to the naked eye, with bands at 487, 542, 581 and 618 nm corresponding to the $^5D_4 \rightarrow {}^7F_J$ transitions (J = 6, 5, 4, 3). The emission intensity of the Eu^{3+} complex is the next brightest, with the Dy^{3+} and Sm^{3+} being the dimmest emitters. The spectra of these complexes show emission bands at 590 and 615 nm for the Eu^{3+} complex ($^5D_0 \rightarrow {}^7F_J$ transitions; J = 1, 2), 478 and 573 nm for the Dy^{3+} complex ($^4F_{9/2} \rightarrow {}^6H_J$ transitions; J = 15/2 and 13/2), and 561, 596 and 643 nm for the Sm^{3+} complex ($^4G_{5/2} \rightarrow {}^6H_J$ transitions; J = 5/2, 7/2 and 9/2). The luminescence spectra of the Ln-**4** complexes in the solid state have similar peaks to those acquired in solutions of acetonitrile, but are broader and less intense (spectra shown in ESI†).

Luminescence lifetimes in acetonitrile are listed in Table 5, and were determined with a 3 : 1 ratio between phosphine oxide **4** and $Ln(NO_3)_3$ to encourage complete metal complexation in solution (2.0 mM complex concentration). The lifetimes below are from fits of the data to a single exponential decay (data shown in ESI†). For these complexes, the lifetime of the Tb^{3+} and Eu^{3+} complexes are longer at 1.77 and 1.43 ms, respectively, than that of the Dy^{3+} and Sm^{3+} complexes, which were measured to be 0.058 and 0.075 ms.

Quantum yields for the four $Ln(NO_3)_3$-**4** complexes, again in the presence of three equivalents of ligand **4**, were determined using the established one-point method[27] (Table 5) using quinine sulfate as the reference standard. We were concerned about complex stability at the low concentrations we needed to work in to acquire spectra with absorption values of less than 0.1, however the NMR dilution data presented in Fig. 4 demonstrates that the complex is still assembled at the concen-

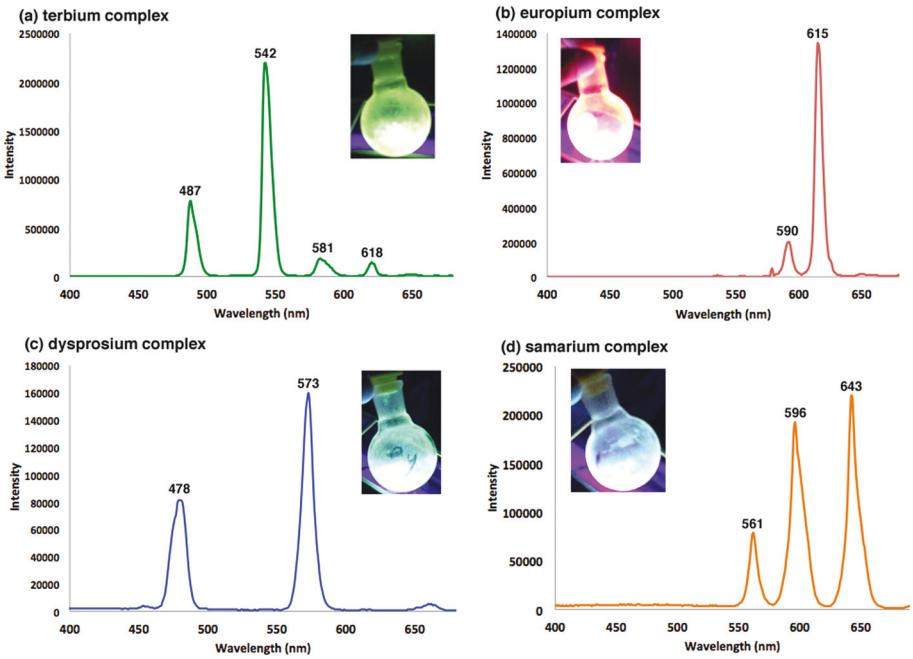

Fig. 7 Uncorrected emission spectra of solutions of 1 : 3 $Ln(NO_3)_3$-**4** in CH_3CN (2.0 mM complex in acetonitrile, excitation = 350 nm) along with photos of the emission from the solid state illuminated using a handheld UV lamp (254 nm). Slit widths (both excitation and emission) were set at 1.0 nm for the spectra of the Tb^{3+}, Dy^{3+} and Eu^{3+} complexes, and 2.0 nm for the spectrum of the Sm^{3+} complex.

Table 5 Emission lifetimes and quantum yield values for 1 : 3 $Ln(NO_3)_3$-**4** complexes excited at 350 nm in acetonitrile. The error bars on both lifetime and quantum yield values represent the standard deviation from three trials

$Ln(NO_3)_3$ complex	τ_{ACN}/ms	Φ_{rel} (%)
Tb	1.77 ± 0.03 (at 545 nm)	14 ± 1
Eu	1.43 ± 0.09 (at 620 nm)	3.9 ± 0.4
Dy	0.058 ± 0.003 (at 580 nm)	0.7 ± 0.1
Sm	0.075 ± 0.006 (at 600 nm)	1.0 ± 0.5

Table 6 Lifetime data of the $Eu(NO_3)_3$-**4** complex in CH_3OH and CH_3OD (2.0 mM), and approximation of the number of bound solvent molecules, *q*. The lifetime values below are averages with standard deviations from three trials, and the *q* value is reported with an error bar of ±0.5 solvent molecules as suggested by Horrocks[44]

	CH_3OH	CH_3OD	*q*
τ/ms at 591 nm	0.3689 ± 0.0009	1.46 ± 0.01	4.3 ± 0.5
τ/ms at 619 nm	0.375 ± 0.001	1.46 ± 0.02	4.2 ± 0.5

trations used to determine these quantum yields (~10^{-5} M). As suggested by the visible results and emission spectra described above, the quantum yield in acetonitrile for the Tb^{3+} complex was the highest at 14% while the Eu^{3+}, Sm^{3+} and Dy^{3+} complexes were less efficient with quantum yield values of 3.9, 1.0 and 0.7%, respectively. We note here that the quantum yields of about 1% for the Sm^{3+} and Dy^{3+} complexes are respectable for these relatively poor emitters.[39–43]

To gain further insight into the solution structure of these complexes, we carried out analysis of the $Eu(NO_3)_3$-**4** complex with three equivalents of ligand **4** in methanol to probe the number of bound solvent molecules.[6,44,45] Lifetime values for this complex were measured at two emission wavelengths, 591 and 619 nm (with excitation at 350 nm), to give nearly identical values when fit to a single exponential decay (Table 6). Analysis of the data shown with the Horrocks equation[44] [$q = 2.1(\tau^{-1}_{MeOH} - \tau^{-1}_{MeOD})$] results in an estimate of 4.3 ± 0.5 and 4.2 ± 0.5 bound solvent molecules (*q*) in solution for the 591 nm and 619 nm emission wavelengths, respectively. These values are interpreted as weighted averages of all of the Eu^{3+} coordination environments present in solution, and suggest a significant degree of inner sphere solvent coordination where the ligands are replaced by the strongly coordinating MeOH solvent. This is unlike what is seen in the solid state and in CH_3CN, based on comparisons of emission intensity.

Low temperature fluorescence and phosphorescence spectra of the 1 : 3 $Gd(NO_3)$-**4** complex at 77 K in acetonitrile were obtained in order to determine the triplet energy of the ligand, and to investigate the relationship between ligand-to-metal energy transfer and resultant Ln emission (Fig. 8). Given the similarities in these spectra, and the shoulder of the excitation peak partially overlapping with the lowest wavelength emission peak at ~405 nm, no clearly discernable singlet-only emission was identified in the fluorescence spectrum. The low temperature phosphorescence spectrum still shows the same peak near 405 nm; this band was assigned as the highest energy emission from the excited ligand triplet state. Shown in Fig. 9, spectral deconvolution of the phosphorescence spectrum was accomplished using a model with five Gaussian dis-

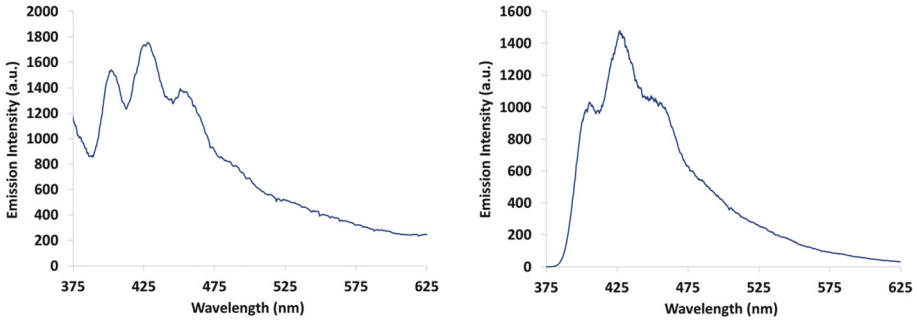

Fig. 8 Fluorescence (left) and phosphorescence (right) spectra of the $Gd(NO_3)_3$-**4** complex with three equivalents of ligand in acetonitrile at 77 K ($[Gd(\mathbf{4})_3(NO_3)_3] = 1 \times 10^{-4}$ M, $\lambda_{ex} = 350$ nm).

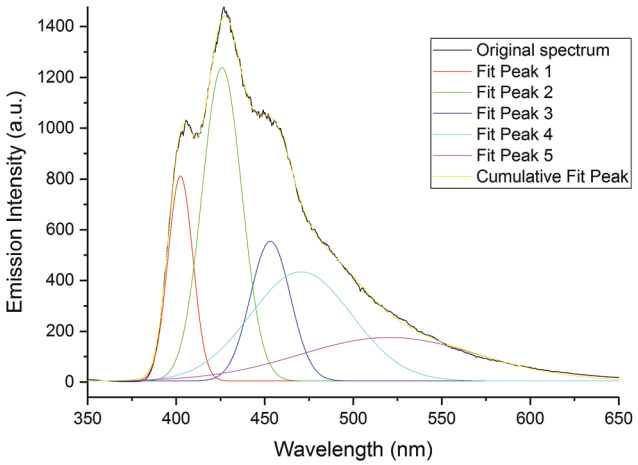

Fig. 9 Spectral deconvolution of the 77 K phosphorescence spectrum of 1 : 3 $Gd(NO_3)_3$-**4** in acetonitrile, modeled with five Gaussian distributions.

tributions to match the number of apparent vibrational bands noted upon visual inspection. Deconvolution of the spectrum into its vibrational components yielded a band at 402 nm, which was used to calculate a ligand triplet state energy of 24 900 cm^{-1}. This energy state for β-ketophosphine oxide **4** is well positioned to facilitate transfer to Tb^{3+} and Dy^{3+} with resonance levels of 20 450 and 20 950 cm^{-1}, respectively, based on the match of ligand triplet state with the primary metal emitting states.[29,38] The much higher quantum yield measured for the Tb^{3+} *versus* Dy^{3+} complex is further explained by the relatively large energy gap between the metal emitting state of Tb^{3+} and lower energy vibrational levels which favors radiative decay and decreases the chances of the many competing non-radiative processes available for Dy^{3+}.[29]

Conclusions

The Ln-coordination chemistry of a bidentate, β-ketophopshine oxide ligand was characterized here in both solution and the solid-state. X-ray crystallographic analysis reveals the presence of multiple Ln-ligand coordination geometries and stoichiometries, depending on the identity of the Ln metal. Of special interest is the report of two different coordination geometries for this ligand with $Eu(NO_3)_3$ in the solid-state. This β-ketophosphine oxide ligand was also able to act as an antenna for the metal-centered luminescence of Eu^{3+}, Tb^{3+}, Sm^{3+} and Dy^{3+}. It is clear from the X-ray crystallographic, IR and NMR data that the functional group of compound **4** that is most responsible for binding to the Ln^{3+} metal center is the phosphine oxide, likely due to its stronger dipole moment across the P═O bond compared to a C═O bond. It is unclear at this point which functional group, the aryl phosphine oxide or the aryl ketone, is responsible for the favorable triplet state energy that renders compound **4** a suitable antenna for sensitization of lanthanide luminescence. Studies toward this end, *via* the preparation of derivatives of compound **4** that possess alkyl groups in place of the aromatic rings, are currently underway.

Abbreviations

Ln	Lanthanide
CMPO	Carbamoylmethylphosphine oxide
TRUEX	Transuranium extraction
LR-ESI MS	Low resolution electrospray ionization mass spectrometry

Conflicts of interest

There are no conflicts to declare.

Acknowledgements

We are grateful to the National Science Foundation for instrumentation and student support (CCLI CHE-0087655, 300 MHz JEOL NMR; MRI CHE-1725699, 400 MHz NMR; REU CHE-1559886, E. Leach), as well as GVSU (OURS, CSCE, Chemistry Department Weldon Fund) and The University of Tampa for financial support. We especially thank the GVSU CLAS Dean's Office for the purchase of the Horiba Fluormax 4

Spectrophotometer. We also thank Pfizer, Inc. for the generous donation of a 400 MHz Varian NMR. We thank Dr George McBane (GVSU) for helpful discussions, Dr Randy Winchester and Prof. James Krikke (GVSU) for help with instrumentation, Dr Tom Guarr, Nick Boersma and Kevin Olson (MSU Bioeconomy Institute) for help determining quantum yields and ESI-MS data, and Dr David Leonard (GVSU) for loaning our group quartz cuvettes. We are grateful to Dr Ana de Bettencourt-Dias and Katherine Johnson (Univ. of Nevada-Reno) for helpful conversations and advice regarding luminescence experiments. All instruments at Michigan State University were purchased or upgraded using departmental funds.

References

1 K. Binnemans, Lanthanide-Based Luminescent Hybrid Materials, *Chem. Rev.*, 2009, **109**, 4283–4374.
2 S. V. Eliseeva and J.-C. G. Bünzli, Lanthanide Luminescence for Functional Materials and Bio-sciences, *Chem. Soc. Rev.*, 2010, **39**, 189–227.
3 G. Wang, Q. Peng and Y. Li, Lanthanide-doped Nanocrystals: Synthesis, Optical-Magnetic Properties, and Applications, *Acc. Chem. Res.*, 2010, **44**, 322–332.
4 C. Spangler and M. Schäferling, Luminescent Chemical and Physical Sensors Based on Lanthanide Complexes, in *Lanthanide Luminescence: Photophysical, Analytical and Biological Aspects*, ed. P. Hänninen and H. Härmä, Springer Heidelberg, Dordrecht, London, New York, 2011, p. 400.
5 D. A. Atwood, *The Rare Earth Elements: Fundamentals and Applications*, John Wiley & Sons Ltd, Chichester, 1st edn, 2012.
6 A. de Bettencourt-Dias, *Luminescence of Lanthanide Ions in Coordination Compounds and Nanomaterials*, Wiley, Chichester, 1st edn, 2014, p. 384.
7 P. Escribano, B. Julián-López, J. Planelles-Aragó, E. Cordoncillo, B. Viana and C. Sanchez, Photonic and nanobiophotonic properties of luminescent lanthanide-doped hybrid organic–inorganic materials, *Mater. Chem.*, 2008, **18**, 23–40.
8 L. D. Carlos, R. A. S. Ferreira, V. de Zea Bermudez and S. J. Ribeiro, Lanthanide-containing light-emitting organic-inorganic hybrids: a bet on the future, *Adv. Mater.*, 2009, **21**, 509–534.
9 J.-C. G. Bünzli, Lanthanide Luminescent Bioprobes (LLBs), *Chem. Lett.*, 2009, **38**, 104–109.
10 A. Thibon and V. C. Pierre, Principles of Responsive Lanthanide-Based Luminescent Probes, *Anal. Bioanal. Chem.*, 2009, **394**, 107–120.
11 J.-C. G. Bünzli, Lanthanide Luminescence for Biomedical Analyses and Imaging, *Chem. Rev.*, 2010, **110**, 2729–2755.
12 M. L. Cable, D. J. Levine, J. P. Kirby, H. B. Gray and A. Ponce, Luminescent Lanthanide Sensors, *Adv. Inorg. Chem.*, 2011, **63**, 1–45.
13 Y. Liu, D. Tu, H. Zhu and E. Ma, Lanthanide-doped Luminescent Nano-bioprobes: From Fundamentals to Biodetection, *Nanoscale*, 2013, **5**, 1369–1384.
14 D. Parker, Luminescent Lanthanide Sensors for pH, pO_2 and Selected Anions, *Coord. Chem. Rev.*, 2000, **205**, 109–130.
15 N. Haque, A. Hughes, S. Lim and C. Vernon, Rare Earth Elements: Overview of Mining, Mineralogy, Uses, Sustainability and Environmental Impact, *Resources*, 2014, **3**, 614–635.
16 E. P. Horwitz, D. C. Kalina, H. Diamond, G. F. Vandegrift and W. W. Schulz, The TRUEX Process - A Process for the Extraction of the Transuranic Elements from Nitric Acid Wastes Utilizing Modified PUREX Solvent, *Solvent Extr. Ion Exch.*, 1985, **3**, 75–109.
17 R. Babecki, A. W. G. Platt and J. Fawcett, Structures of Lanthanide Complexes of b-Ketophosphoryl Compounds, *J. Chem. Soc., Dalton Trans.*, 1992, 675–681.
18 R. Babecki, A. W. G. Platt and D. R. Russell, Synthesis of cerium(III) and (IV) complexes of phenacyldiphenylphosphine oxide. The structure of Ce(NO3)3[Ph2P(O)CH2C(O)Ph]3, *Inorg. Chim. Acta*, 1990, **171**, 25–28.
19 R. Babecki, A. W. G. Platt, J. C. Tebby, J. Fawcett, D. R. Russell and R. Little, The crystal and molecular structure of UO2(NO3)2[Ph2P(O)CH2C(O)Ph]2 and its role in the solvent extraction of the uranyl ion, *Polyhedron*, 1989, **8**, 1357–1360.
20 *COSMO v1.61 Software for the CCD detector systems for determining data collection parameters*, Bruker Analytical X-ray Systems, Madison, WI, 2009.
21 *APEX2 v2010.11-3 Software for the CCD detector system*, Bruker Analytical X-ray Systems, Madison, WI, 2010.
22 *SAINT v7.68A Software for the Integration of CCD Detector System*, Bruker Analytical X-ray Systems, Madison, WI, 2010.
23 R. H. Blessing, SADABS v2.008/2 Program for absorption correction using Bruker-AXS CCD based on the method of Robert Blessing, *Acta Crystallogr., Sect. A: Fundam. Crystallogr.*, 1995, **51**, 33–38.
24 G. M. Sheldrick, A short history of SHELX, *Acta Crystallogr., Sect. A: Fundam. Crystallogr.*, 2008, **64**, 112–122.
25 O. V. Dolomanov, L. J. Bourhis, R. J. Gildea, J. A. K. Howard and H. Puschmann, OLEX2: a complete structure solution, refinement and analysis program, *J. Appl. Crystallogr.*, 2009, **42**, 339–341.
26 L. J. Bourhis, O. V. Dolomanov, R. J. Gildea, J. A. K. Howard and H. Puschmann, The anatomy of a comprehensive constrained, restrained, refinement program for the modern computing environment - Olex2 dissected, *Acta Crystallogr., Sect. A: Fundam. Crystallogr.*, 2015, **71**, 59–75.
27 C. A. Parker and W. T. Rees, Correction of Fluorescence Spectra and Measurement of Fluorescence Quantum Yield, *Analyst*, 1960, **85**, 587–600.
28 D. Nagaraja, R. M. Melavanki, N. R. Patil and R. A. Kusanur, Solvent effect on the relative quantum yield and fluorescence quenching of 2DAM, *Spectrochim. Acta, Part A*, 2014, **130**, 122–128.
29 G. A. Crosby, R. E. Whan and R. M. Alire, Intramolecular energy transfer in rare earth chelates. Role of the triplet state, *J. Chem. Phys.*, 1961, **14**, 743–748.

30 T. Shintou, W. Kikuchi and T. Mukaiyama, Efficient Method for the Preparation of Carboxylic Acid Alkyl Esters or Alkyl Phenyl Ethers by a New-Type of Oxidation-Reduction Condensation Using 2,6-Dimethyl-1,4-benzoquinone and Alkoxydiphenylphosphines, *Bull. Chem. Soc. Jpn.*, 2003, **76**, 1645–1667.

31 F. Arnaud-Neu, V. Böhmer, J.-F. Dozol, C. Grüttner, R. A. Jakobi, D. Kraft, O. Mauprivez, H. Rouquette, M.-J. Schwing-Weill, N. Simon and W. Vogt, Calixarenes with diphenylphosphoryl acetamide functions at the upper rim. A new class of highly efficient extractants for lanthanides and actinides, *J. Chem. Soc., Perkin Trans. 2*, 1996, 1175–1182.

32 E. M. Schuster, G. Nisnevich, M. Botoshansky and M. Gandelman, Synthesis of Novel Bulky, Electron-Rich Propargyl and Azidomethyl Dialkyl Phosphines and Their Use in the Preparation of Pincer Click Ligands, *Organometallics*, 2009, **28**, 5025–2031.

33 P. van der Sluis and A. L. Spek, BYPASS: an effective method for the refinement of crystal structures containing disordered solvent regions, *Acta Crystallogr., Sect. A: Fundam. Crystallogr.*, 1990, **46**, 194–201.

34 W. T. Carnall, S. Siegel, J. R. Ferraro, B. Tani and E. Gebert, New series of anhydrous double nitrate salts of the lanthanides. Structural and spectral characterization, *Inorg. Chem.*, 1973, **12**, 560–564.

35 D. S. Kumar and V. Alexander, Macrocyclic complexes of lanthanides in identical ligand frameworks part 1. Synthesis of lanthanide(III) and yttrium(III) complexes of an 18-membered dioxatetraaza macrocycle, *Inorg. Chim. Acta*, 1995, **238**, 63–71.

36 V. A. J. Aruna and V. Alexander, Synthesis of lanthanide(III) complexes of a 20-membered hexaaza macrocycle, *J. Chem. Soc., Dalton Trans.*, 1996, 1867–1873.

37 S. I. Weissman, Intramolecular Energy Transfer: The Fluorescence of Complexes of Europium, *J. Chem. Phys.*, 1942, **10**, 214–217.

38 J.-C. G. Bünzli, On the design of highly luminescent lanthanide complexes, *Coord. Chem. Rev.*, 2015, **293–294**, 19–47.

39 Z. Darzynkiewicz, E. Holden, A. Orfao, W. G. Telford and D. Wlodkowic, *Recent advances in cytometry, Part A: Instrumentation, methods*, Elsevier, Oxford, UK, 5th edn, 2011, vol. 102.

40 I. Hemmilä and V. Laitala, Progress in lanthanides as luminescent probes, *J. Fluoresc.*, 2005, **15**, 529–542.

41 A. T. Bui, A. Grichine, S. Brasselet, A. Duperray, C. Andraud and O. Maury, Unexpected efficiency of a luminescent Sm (III) complex for combined visible and near-infrared biphotonic microscopy, *Chem. – Eur. J.*, 2015, **21**, 17757–17761, DOI: 10.1002/chem.201503711.

42 W.-S. Lo, J. Zhang, W.-T. Wong and G.-L. Law, Highly luminescent Sm(III) complexes with intraligand charge-transfer sensitization and the effect of solvent polarity on their luminescent properties, *Inorg. Chem.*, 2015, **54**, 3725–3727, DOI: 10.1021/acs.inorgchem.5b00331.

43 S. Biju, Y. K. Eom, J.-C. G. Bünzli and H. K. Kim, A new tetrakis beta-diketone ligand for NIR emitting Ln(III) ions: luminescent doped PMMA films and flexible resins for advanced photonic applications, *J. Mater. Chem. C*, 2013, **1**, 6935–6944, DOI: 10.1039/C3TC31181C.

44 R. C. Holz, C. A. Chang and W. D. Horrocks, Spectroscopic characterization of the europium(III) complexes of a series of N,N'-bis(carboxymethyl) macrocyclic ether bis(lactones), *Inorg. Chem.*, 1991, **30**, 3270–3275.

45 R. M. Supkowski and W. D. Horrocks Jr., On the determination of the number of water molecules, q, coordinated to europium(III) ions in solution from luminescence decay lifetimes, *Inorg. Chim. Acta*, 2002, **340**, 44–48.